JACS
JOURNAL OF THE AMERICAN CHEMICAL SOCIETY

Article

pubs.acs.org/JACS

Toward the Design of Smart Delivery Systems Controlled by Integrated Enzyme-Based Biocomputing Ensembles

Paula Díez,[†] Alfredo Sánchez,[†] María Gamella,[†] Paloma Martínez-Ruíz,[‡] Elena Aznar,[§,∥] Cristina de la Torre,[§,∥] José R. Murguía,[§,∥] Ramón Martínez-Máñez,*[,§,∥] Reynaldo Villalonga,*[,†,⊥] and José M. Pingarrón*[,†,⊥]

Departments of [†]Analytical Chemistry and [‡]Organic Chemistry I, Faculty of Chemistry, Complutense University of Madrid, 28040 Madrid, Spain

[§]Instituto de Reconocimiento Molecular y Desarrollo Tecnológico (IDM), Centro Mixto Universitat Politècnica de València—Universitat de València, 46022 Valencia, Spain

[∥]Departamento de Química and CIBER de Bioingeniería, Biomateriales y Nanomedicina (CIBER-BBN), Universitat Politècnica de València, 46022 Valencia, Spain

[⊥]IMDEA Nanoscience, City University of Cantoblanco, 28049 Madrid, Spain

Supporting Information

ABSTRACT: We report herein the design of a smart delivery system in which cargo delivery from capped mesoporous silica (MS) nanoparticles is controlled by an integrated enzyme-based "control unit". The system consists of Janus-type nanoparticles having opposing Au and MS faces, functionalized with a pH-responsive β-cyclodextrin-based supramolecular nanovalve on the MS surface and two effectors, glucose oxidase and esterase, immobilized on the Au face. The nanodevice behaves as an enzymatic logical OR operator which is selectively fueled by the presence of D-glucose and ethyl butyrate.

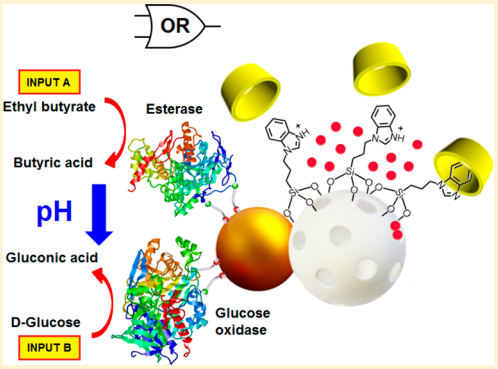

INTRODUCTION

Evolution in biomolecular chemistry combined with nanotechnology has recently resulted in the design of biologically based systems with innovative functions.[1] A significant issue in this field has been the development of new "intelligent" devices using nanoscopic structures and a variety of biomolecules, fueling areas such as bioengineering, biosensing, and drug delivery. In this context, the design of smart delivery systems that are able to release entrapped guests in a controlled fashion has received great attention in recent years. The advent of nanotechnology has provided a large variety of novel nanomaterials which have found application in this area.[3] Mesoporous silica (MS) supports have been widely explored as promising alternatives for delivery uses due to their large specific volume, large loading capacity, low cost, and low toxicity.[4] An interesting characteristic of these MS nanoparticles is that they can be rationally functionalized with molecular or supramolecular ensembles on their external surface to develop gated nanocarriers showing "zero delivery",[5] which can further release their cargo in response to target physical (such as light, temperature, or magnetic fields),[6] chemical (such as pH changes, redox-active molecules, or selected anions),[7] and biochemical (such as enzymes, antibodies, or DNA) stimuli.[8]

However, in most of these systems, the effector (i.e., the agent that regulates the delivery activity) is external to the delivery nanoparticle, a fact that somehow limits the design of "smart" nanodevices for delivery applications. A way to overcome this restriction is to design nanosupports in which the gating system and the effector molecule are integrated in the same nanodevice.[9] In this approach, one can envision the design of a "control unit" attached to the gated nanoparticle in which one or several agents that regulate the delivery activity are placed (see Scheme 1). The role of this unit is to handle the chemical information (input) of the environment and transform it (via the use of the effectors) into new chemicals that control the state of the gate (open or closed). This strategy can also promote effective protection to the effectors, such as enzymes, due to immobilization, which ensures their functionality when they reached the target place.

Moreover, the possibility of using a combination of different effectors in the "control unit" opens new perspectives in the development of complex systems that can generate specific results (delivery or not, control of the delivery kinetics, etc.) via

Received: April 10, 2014
Published: June 6, 2014

   dx.doi.org/10.1021/ja503578b | J. Am. Chem. Soc. 2014, 136, 9116−9123

Scheme 1. Schematic Representation of "Smart" Delivery Systems Containing an Attached Control Unit That Regulates the Delivery Activity of the Gated Material

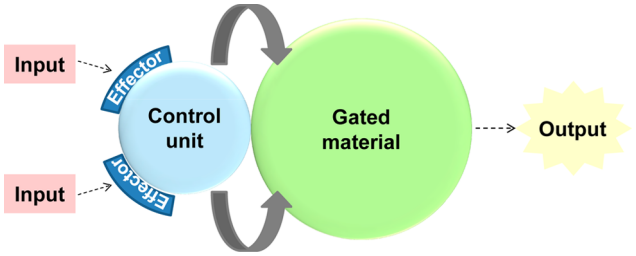

logical operations based on different chemical inputs. However, as far as we know, such engineered release systems have not been described.

Chemically speaking, a general strategy toward the integration of the gating system and effectors in the same nanodevice may be the conjugation of two very different nanoparticles having different surfaces and well-defined and specific functionalization chemistries. As a suitable approach for this goal, Janus nanoparticles are especially appropriate.[10] Following this general concept, and as proof-of-concept, we report herein the design of Janus gold-MS nanoparticles[9] in which the gated ensemble in the MS face is combined with one or more effectors placed on the gold side of the Janus support. The proposed design involves the immobilization of two enzymes, glucose oxidase (EC 1.1.3.4) and esterase (EC 3.1.1.1), on the gold face as effectors, with the cargo release governed by an enzymatic logical OR operator (see Figure 1). Moreover, the MS face of the Janus nanoparticles is used as a nanocontainer for cargo loading and equipped with a pH-responsive β-cyclodextrin-based supramolecular nanovalve.[7f,11]

The Au side is expected to act as the "control unit", in which the enzyme effectors would interpret the presence of specific chemical inputs (enzyme substrates) and would direct the operation (cargo delivery) of the system. In particular, we envisioned that the gated mesoporous nanodevice will show "zero-release" yet will open selectively in the presence of either D-glucose or ethyl butyrate, or a combination of both substrates, through enzyme-catalyzed substrate transformations which will lead to a reduction of the pH and, consequently, to the opening of the β-cyclodextrin-gated nanovalves. The overall output (cargo delivery) will function as a Boolean logic OR gate.[12]

RESULTS AND DISCUSSION

To assemble the integrated nanomachine, Janus Au-MS nanoparticles were first prepared as previously described.[9,13] The synthetic procedure is based on the manipulation of the Au–ligand–MS interface through a mask-protecting assisted site-selective modification approach. Briefly, MS nanoparticles (**S0**, average diameter: 97 ± 15 nm) were synthesized by alkaline hydrolysis of tetraethyl orthosilicate as inorganic precursor in the presence of the cationic surfactant cetyltrimethylammonium bromide as porogen species. Subsequent removal of the surfactant by calcination in air at high temperature resulted in the starting mesoporous inorganic support. These nanoparticles were then partially confined at the interface of a Pickering emulsion using paraffin wax as the oil phase. The exposed nanoparticle surface was further modified with (3-mercaptopropyl)trimethoxysilane on which Au nanoparticles (average diameter: 20 ± 2 nm) were then attached, yielding stable anisotropic colloids (**S1**, average diameter: 104 ± 17 nm, yield 85%) after the paraffin wax was dissolved in $CHCl_3$.

The MS nanoparticles in the anisotropic colloids were then loaded with $Ru(bipy)_3^{2+}$, which was used as a dye for monitoring the release process, and the external surface of the siliceous face was further modified with 3-iodopropyltrimethoxysilane. Benzimidazole moieties were attached to the anchored 3-iodopropyl residues through a nucleophilic substitution reaction, yielding a solid functionalized with 1-propyl-1*H*-benzimidazole groups (**S2**). These nanoparticles were then gated with a pH-sensitive supramolecular nanovalve by stirring the colloid with β-cyclodextrin moieties in water at pH 7.5 for 24 h, which resulted in the formation of inclusion complexes between the benzimidazole groups and the β-

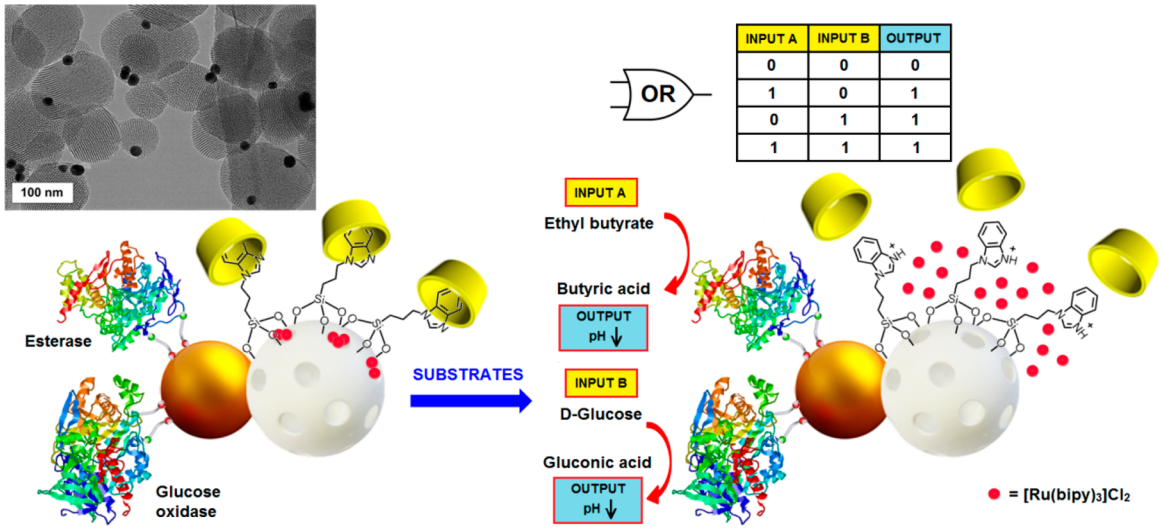

Figure 1. Performance of the Janus-based nanodevice **S3**. The "control unit" (Au face) is functionalized with two effectors (enzymes), which control cargo delivery from the mesoporous silica face via interpretation of different chemical inputs (D-glucose, ethyl butyrate). Overall, the system functions as an enzymatic logical OR operator.

dx.doi.org/10.1021/ja503578b | J. Am. Chem. Soc. 2014, 136, 9116–9123

cyclodextrins.[7f,11] Finally, esterase and glucose oxidase, previously modified with 3,3′-dithiobis(sulfosuccinimidyl-propionate), were selectively and covalently immobilized on the Au face of the **S2** colloid by incubation in 50 mM sodium phosphate buffer, pH 7.5, at 4 °C, yielding the final nanodevice **S3**.

Au nanoparticles were selected as the scaffold for the assembly of the effector system, instead of using direct enzyme immobilization on the MS surface. This choice was based on the large surface area of Au nanoparticles, which allows high enzyme loadings with the immobilization method employed. In addition, the relatively low Au reactivity allows the metal nanoparticles surface to remain unaltered during the further assembly of the gated system in the MS face, thus avoiding chemical protection steps that should be employed to directly link the enzymes to the MS face.

All supports were characterized by standard methods (see Supporting Information (SI)). Transmission electron microscopy (TEM) analysis confirmed the mesoporous morphology of the silica nanoparticles as well as the presence of the Au nanoparticles in the Janus colloids (Figure 1). Powder X-ray diffraction (PXRD) patterns of the final nanodevice **S3** and the intermediate **S0**, **S1**, and **S2** supports are shown in Figure SI-1. All samples showed a well-defined low-angle reflection around 2.6°, which corresponds to a hexagonal ordered array indexed as a (100) Bragg peak, suggesting an MCM41-like mesoporous order in these materials which was not affected by the different chemical modifications and dye loading processes. In addition, the diffraction patterns of **S1**, **S2**, and **S3** samples at high angle also showed the cubic gold characteristic (111), (200), (220), and (311) diffraction peaks,[14] confirming the Janus Au-MS architecture observed by TEM. The Fourier transform infrared (FT-IR) spectra of the **S0** and **S1** nanoparticles were similar to those reported for MS and Janus Au-MS nanoparticles, whereas the characteristic IR absorption bands of benzimidazole were clearly observed in the spectrum of **S2** (Figure SI-2).[15] On the other hand, the presence of *β*-cyclodextrin moieties in **S3** was confirmed by the broad band at ca. 1060 cm^{-1}, which is characteristic for this cyclic oligosaccharide. The presence of the immobilized enzymes in **S3** was confirmed by the band at 1642 cm^{-1}, which can be ascribed to the amide I absorption band of proteins. Moreover, thermogravimetric (Figure SI-3) and elemental analysis studies (Table SI-1) on **S1**, **S2**, and **S3** revealed the content of the $Ru(bpy)_3^{2+}$ dye and anchored benzimidazole in **S2** to be 15 and 160 *μ*mol/g, respectively. In addition, the amount of glucose oxidase and esterase immobilized on **S3** was estimated to be 2.5 and 4.8 U/mg, respectively.

The N_2 adsorption−desorption isotherms of the starting calcined MS nanoparticles (**S0**) and the Janus colloid (**S1**) showed an adsorption step at intermediate P/P_0 values (0.1−0.3). Application of the BET model for these solids resulted in values for the total specific surface area of 1037 and 819 $m^2\ g^{-1}$, respectively (see Figure SI-4 and Table SI-2). In contrast, the N_2 adsorption−desorption isotherms for the prepared dye-loaded material (**S2**) and the final capped support (**S3**) are typical of mesoporous systems with filled mesopores, and a significant decrease in the N_2 volume adsorbed and surface area was observed (i.e., 51.3 and 18.2 $m^2\ g^{-1}$ for **S2** and **S3**, respectively, see SI).[7f]

The capacity of the **S3** nanodevice to deliver the cargo in aqueous solution was further tested. In a typical release assay, 10 mg of **S3** was suspended in 4 mL of 20 mM Na_2SO_4 solution at pH 7.5 and shaken over time at 25 °C. Aliquots were taken at scheduled times and centrifuged to remove the nanoparticles, and then the absorbance at 454 nm of the released $Ru(bpy)_3^{2+}$ was measured. After 1 h incubation, the enzyme substrates D-glucose and ethyl butyrate, used as input signals, were added to the mixtures at a concentration of 40 *μ*M.

Figure 2 shows the time course of $Ru(bpy)_3^{2+}$ release from the pores of **S3** nanoparticles in the presence and absence of

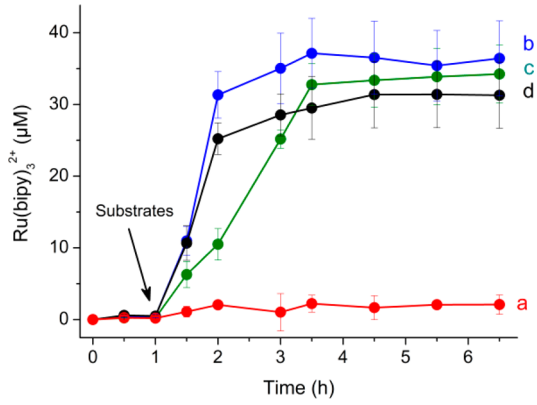

Figure 2. Kinetics of dye release from **S3** in 20 mM Na_2SO_4, pH 7.5, in the absence (a) and the presence of 40 *μ*M ethyl butyrate (b), D-glucose (c), and ethyl butyrate + D-glucose (d). Substrates were added after 1 h of incubation.

substrates. In the absence of D-glucose or ethyl butyrate solid, **S3** is tightly capped and shows a negligible release of $Ru(bpy)_3^{2+}$ (ca. 1.2 ± 0.5 *μ*M $Ru(bpy)_3^{2+}$, see curve a). In contrast, the presence of either ethyl butyrate (curve b) or D-glucose (curve c), or a mixture of both (curve d), results in the opening of the pores and subsequent release of the cargo. Overall, delivery from **S3** nanoparticles is triggered by the presence of ethyl butyrate and D-glucose via the "interpretation" of these chemical inputs by the glucose oxidase and esterase enzymes (effectors) in the "control unit" that resulted in the dethreading of the inclusion complex between benzimidazole moieties and *β*-cyclodextrin. In particular, glucose oxidase catalyzed the oxidation of D-glucose, yielding H_2O_2 and D-glucono-1,5-lactone, which hydrolyzes in water to gluconic acid (pK_a = 3.6). Moreover, ethyl butyrate is catalytically hydrolyzed by esterase enzyme to ethanol and butyric acid (pK_a = 4.82). Both catalytic reactions result in a reduction in the pH of the incubation solutions, causing the protonation of benzimidazole moieties (pK_a = 5.55)[16] on the MS face of **S3**, dethreading of the inclusion complex, and cargo delivery.

As illustrated in Figure 2, the esterase-mediated process showed faster delivery kinetics than those mediated by glucose oxidase, reaching plateau values of about 36.1 ± 0.8 and 33.5 ± 0.6 *μ*M $Ru(bpy)_3^{2+}$ after 2 and 2.5 h of addition of the corresponding substrates, respectively. This difference in the released dye is tentatively ascribed to the lower amount of glucose oxidase immobilized on Au nanoparticles. In addition, glucose oxidase has a more acidic optimum pH range (pH 4−7, with maximum at pH 5.5) than that for esterase (pH 6−9, with maximum at pH 8.0),[17] which results in a lower catalytic activity for glucose oxidase, especially at the beginning of the reaction.

Moreover, to demonstrate that the opening mechanism was due to the enzyme-mediated reduction of pH, it was confirmed

dx.doi.org/10.1021/ja503578b | J. Am. Chem. Soc. 2014, 136, 9116−9123

that, in the experiments in which ethyl butyrate or D-glucose were added to aqueous suspensions of **S3**, the pH of the incubating medium changed from 8.0 to ca. 5.0 after 6 h. In addition, in order to demonstrate that it is the presence of the glucose oxidase and esterase enzymes in the Au "control unit" that governed cargo delivery, a suspension of **S3** at pH 7.5 was boiled for 10 min to inactivate the enzymes, and further tested toward D-glucose and ethyl butyrate. In this case, no appreciable cargo delivery was observed from **S3** after 24 h of incubation.

To elucidate whether the release of $Ru(bpy)_3^{2+}$ from the Janus colloid was caused by a local decrease of the pH in the microenvironment of the nanoparticles or by pH decrease in the bulk solution, parallel release experiments in buffered solutions at pH 7.5 were performed. As is exemplified in Figure SI-5, when D-glucose + ethyl butyrate are used as triggers, the concentrations of $Ru(bpy)_3^{2+}$ released at a given time to the buffered solution were only slightly lower than those corresponding to the non-buffered medium. Measurements of the final pH values of the buffered solutions confirmed that no changes were apparent upon for release experiments, suggesting that the enzyme-controlled cargo release from the Janus nanoparticles was mainly provoked by local acidification of the colloid microenvironment caused by the biocatalytic transformation of the trigger enzyme substrates.

The experiments carried out can be summarized in a Boolean-like table (see Figure 1), in which the observed output (delivery (1) or not (0) of the cargo from **S3**) depends on the presence (1) or not (0) of the small molecules D-glucose and ethyl butyrate. Thus, whereas solid **S3** displayed no release (input values 0,0; output value 0), the presence of the enzymes' substrates as input values (0,1; 1,0; 1,1) induced the delivery of the entrapped guest (output value 1). In terms of delivery, **S3** behaves as an enzymatic logical OR operator.

In order to expand the possibilities of the enzyme-controlled nanomachine, a new **S4** nanodevice was synthesized by co-immobilizing also the enzyme urease (Ec 3.5.1.5) on the Janus Au nanoparticles face. Urease catalyzed hydrolysis of urea to CO_2 and NH_3, which resulted in a progressive increase in the pH value of the incubation solutions, this acting as a RESET operator for the pH-mediated release process. Figure 3 (curves b and d, open circles) clearly shows a noticeable decrease in the amount of released dye when urea was also added as a trigger. This effect can be attributed to a partial neutralization of the acidic medium by the ammonia produced through the urease-catalyzed reaction, switching off the opening of the supramolecular nanovalves and thus controlling the dye release. A possible reduction of the glucose oxidase and esterase activity by a local increase of pH should be also considered as a possible mechanism for this urease-based switch-off action.

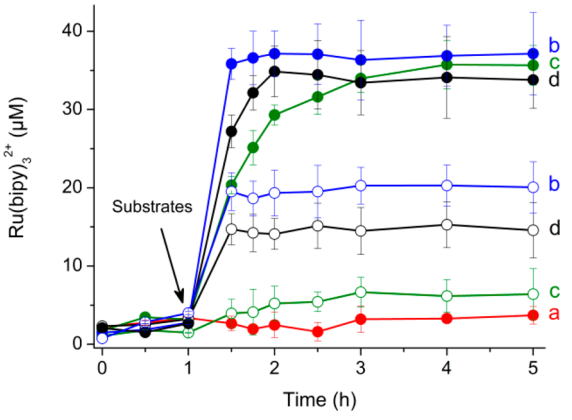

Figure 3. Kinetics of dye release from **S4** in 20 mM Na_2SO_4, pH 7.5, in the absence (a) and the presence of 40 μM ethyl butyrate (b), D-glucose (c), and ethyl butyrate + D-glucose (d) without (closed circles) and with 200 μM urea (open circles). Substrates were added after 1 h of incubation.

Figure 4 shows the effect of the time at which urea was added to the incubation media on the kinetics of dye release from solid **S4** triggered with D-glucose. The concentration of released $Ru(bpy)_3^{2+}$ increased as the time at which urea was introduced into the media was increased, demonstrating that the urease-based RESET operator, and thus the amount of dye released, can be operated through a time-controlled scheme.

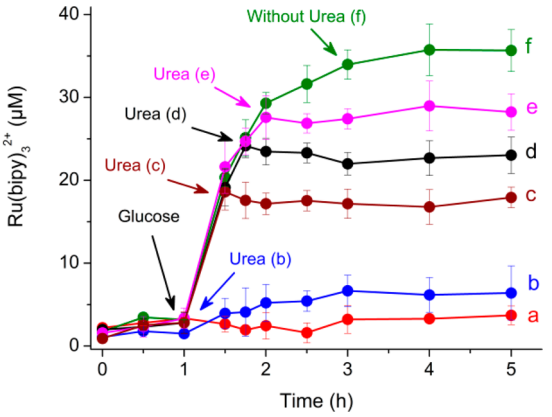

Figure 4. Kinetics of dye release from **S4** in 20 mM Na_2SO_4, pH 7.5, in the absence (a) and the presence of 40 μM D-glucose without (f) and with addition of urea at 200 μM final concentration at different times (b–e). Substrates were added after 1 h of incubation.

One goal of this study was to demonstrate that Janus enzyme-controlled capped MS can be used for in-cell controlled delivery applications. Therefore, after *in vitro* characterization of the solid **S3** (*vide ante*), similar nanoparticles were tested in further *ex vivo* assays. In particular, for these experiments, nanoparticles like **S3** but loaded with the cytotoxic doxorubicin (Doxo) were prepared (solid **S5**, see SI). The amount of Doxo loaded on the Janus colloid was estimated spectrophotometrically as 0.56 μmol per gram of nanoparticles. The **S5** nanomachine showed patterns for *in vitro* Doxo release similar to those of nanoparticles filled with $Ru(bpy)_3^{2+}$ upon addition of ethyl butyrate or D-glucose + ethyl butyrate, but lower release kinetics in the presence of D-glucose (Figure 5).

The **S5** nanomachine retained full functional activity after 1 month of storage at 4 °C. In addition, the operational stability of the **S5** nanomachine was tested by incubation at 37 °C in reconstituted human serum and further quantification of Doxo released 1 h after addition of D-glucose + ethyl butyrate as triggers (see SI for details). As illustrated in Figure SI-6, the integrated nanomachine lost release activity progressively with time according to biphasic inactivation kinetics. However, the **S5** solid retained over 40% of the initial functional activity after 1 week of incubation, suggesting its potential use for long-term *ex vivo* assays.

The solid **S5** was *ex vivo* analyzed in HeLa cells under the premise that **S5** could be internalized by the cells and would remain closed until glucose or ethyl butyrate is added. The

dx.doi.org/10.1021/ja503578b | J. Am. Chem. Soc. 2014, 136, 9116–9123

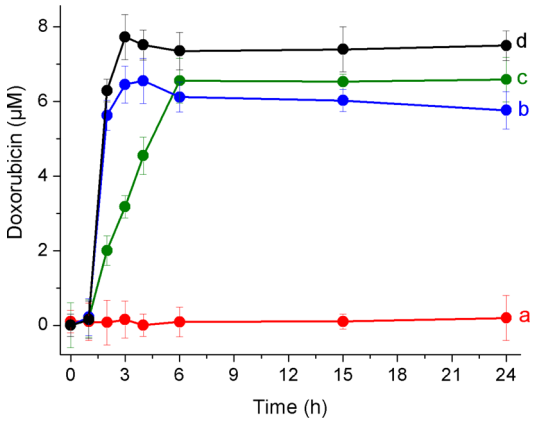

Figure 5. Kinetics of Doxo release from **S5** in 20 mM Na_2SO_4, pH 7.5, in the absence (a) and the presence of 40 μM ethyl butyrate (b), D-glucose (c), and ethyl butyrate + D-glucose (d). Substrates were added after 1 h of incubation.

action of enzymes in the Janus nanoparticle on these molecules would induce a local pH reduction that is expected to result in an intracellular Doxo release, which would induce cell death. In a typical experiment, HeLa cells were incubated for 40 min with a suspension of 100 μg/mL of **S5** in phosphate-buffered saline (PBS) supplemented with 10% fetal bovine serum (FBS). Afterward, cells were washed in order to remove un-internalized nanoparticles and further incubated alone or in the presence of ethyl butyrate (input A), glucose (input B), or a mixture of both (see Methods for details). Delivery of Doxo from **S5** in the presence of the different inputs was first studied by confocal microscopy by tracking Doxo-associated fluorescence. Moreover, in these experiments, the cell nuclei were stained with Hoechst 33342.

Figure 6A shows representative phase contrast images of Doxo, Hoescht, and combined for HeLa cells first loaded with **S5** and then untreated (−/−) or treated with ethyl butyrate (+/−), glucose (−/+), or a mixture of both (+/+). Internalization of **S5** in HeLa cells (see −/−) did not produce, in the absence of further input, a significant Doxo release, thus demonstrating that no unspecific cargo release occurred to a large extent as a consequence of the acidification in the endosomes. In contrast, when cells were incubated simultaneously with ethyl butyrate and glucose, a clear dispersed Doxo fluorescence was found, indicating cargo delivery from **S5**. Figure 6C shows a quantitation using flow cytometry of the Doxo fluorescence intensity for HeLa cells incubated with **S5** (−/−) and further treated with ethyl butyrate (+/−), glucose (−/+), or a mixture of both (+/+). Whereas emission was low in the absence of inputs, an enhanced Doxo fluorescence was detected upon exposure to ethyl butyrate or glucose. Moreover, a synergistic enhanced Doxo emission was observed when ethyl butyrate and glucose treatments were combined simultaneously.

These observations correlate with cell viability studies done after 24 h of the corresponding treatment using WST-1 assays (see Figure 6B). Indeed, it was confirmed that HeLa cells treated at 100 μg/mL of **S5** in the presence of glucose and ethyl butyrate showed apoptotic cell death. More specifically, around 50% of the cells were dead 24 h after the addition of **S5**, whereas values of ca. 40% and 15% of dead cells were found when only glucose or ethyl butyrate was added, respectively. In contrast, the HeLa cells treated with only **S5** remained unaffected.

CONCLUSIONS

In summary, we have demonstrated that it is possible to design nanodevices in which the gating mechanisms and different effector ensembles can be integrated in a unique system. In particular, we report here the preparation of Janus-type nanoparticles having opposing Au and MS faces, functionalized with a pH-responsive β-cyclodextrin-based supramolecular nanovalve on the MS surface and two effectors, glucose oxidase and esterase, immobilized on the Au face. The nanodevice behaves as an enzymatic logical OR operator which is fueled by the presence of D-glucose and ethyl butyrate. This enzyme logic system was also coupled to a urease-based RESET operator to switch-off the opening of the supramolecular nanovalves and control the extent of dye delivery upon addition of urea. To our knowledge, this is the first report dealing with the use of anisotropic colloids for the design of smart nanodevices for on-command release controlled by biochemical logic operations. The smart nanomachine controlled by the logical OR operator and loaded with an anti-cancer drug was successfully tested with HeLa cancer cells. The possibility of using a large variety of different gating nanovalves on the MS face combined with potentially a number of enzyme-based effectors on the Au surface makes this approach appealing and opens a wide range of new possibilities for the development of novel smart delivery systems controlled by enzyme-based biocomputing ensembles.

METHODS

Preparation of MS Nanoparticles (S0).[18] Cetyltrimethylammonium bromide (3.0 g) was dissolved in 1.44 L of water under sonication. NaOH solution (2.0 mol/L, 10.5 mL) was then added, and the temperature of the mixture was adjusted to 80 °C. Tetraethoxysilane (15.0 mL) was added dropwise to the surfactant solution within 5 min under vigorous magnetic stirring. The mixture was allowed to react for 2 h. The resulting white solid was filtered, washed with water and methanol, and then dried in a desiccator. Finally, the solid was calcined at 550 °C for 5 h to remove the organic template.

Preparation of 20 nm Au Nanoparticles.[19] Freshly prepared 3 μM $HAuCl_4$ solution (50 mL) was heated to boiling. Then, 750 μL of a 3.9 μM trisodium citrate solution was added to synthesize 20 nm gold nanoparticles. The mixture was heated for 10 min, cooled to room temperature, and finally diluted to 50 mL with ultrapure water.

Preparation of Janus Au-MS Nanoparticles (S1).[9,13] MS nanoparticles (200 mg) were dispersed homogeneously in 10 mL of 1.0 μM cetyltrimethylammonium bromide in 6.7% ethanol aqueous solution. The mixture was heated at 75 °C, and then 1 g of paraffin wax was added. When the paraffin wax was melted, the mixture was vigorously stirred at 25 000 rpm for 10 min using an Ultra-Turrax T-10 homogenizer (IKA, Germany). The resulting emulsion was further stirred for 1 h at 4000 rpm and 75 °C, using a magnetic stirrer. The resulting Pickering emulsion was then cooled to room temperature, mixed with 10 mL of methanol, and treated with 200 μL of (3-mercaptopropyl)trimethoxysilane. After 3 h under magnetic stirring, the silanized emulsion was filtered, washed three times with methanol, and further dispersed in 400 mL of the corresponding 3 μM Au nanoparticles aqueous solutions. The mixture was stirred overnight and then filtered and exhaustively washed with ultrapure water. The solid was suspended in ethanol, centrifuged, and washed two times with ethanol and three times with chloroform. The Janus nanoparticles were finally dried and kept in desiccators until use.

Preparation of S2. To synthesize **S2**, 400 mg of **S1** and 250 mg (33 μmol) of tris(2,2′-bipyridyl)dichlororuthenium(II) hexahydrate were suspended in 17 mL of anhydrous acetonitrile in a round-bottom flask connected to a Dean−Stark trap under an Ar atmosphere. The

dx.doi.org/10.1021/ja503578b | J. Am. Chem. Soc. 2014, 136, 9116−9123

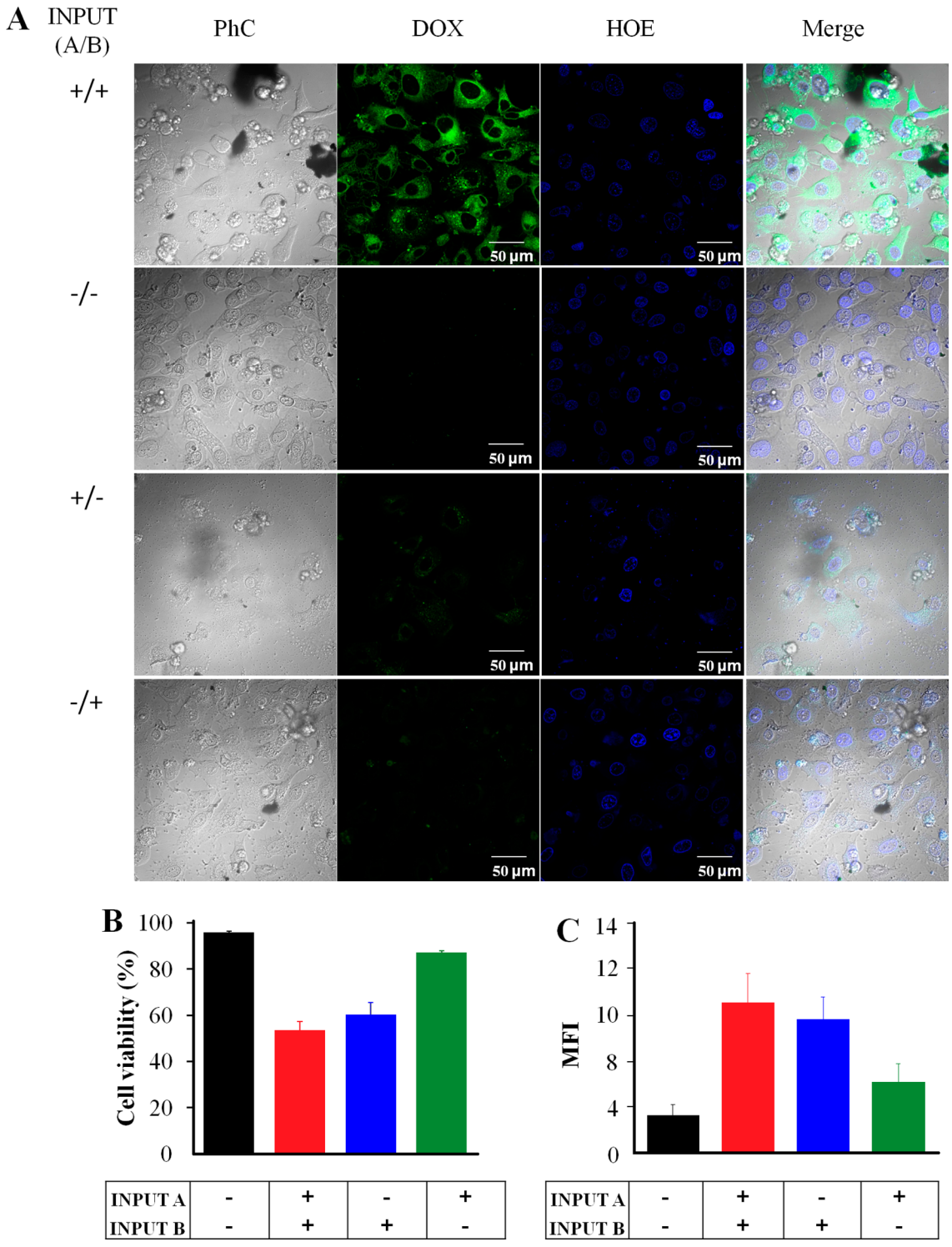

Figure 6. Internalization and release of cargo in HeLa cells. (A) Controlled release of doxorubicin (Doxo)-loaded **S5** nanoparticles in HeLa cells. Cultures were incubated with 100 μg/mL of **S5** in the presence of different inputs and examined for Doxo by confocal microscopy. Representative phase contrast images at 24 h from (PhC), Doxo (DOX), Hoescht (HOE), and combined (Merge) are shown. (B) Cell viability test of 150 μg/mL concentration of **S5** with glucose and/or ethyl butyrate at 24 h in HeLa cells using WST-1 assay. (C) Quantification of Doxo fluorescence intensity by flow cytometry in cells under different conditions. Ethyl butyrate treatment (input A)/glucose treatment (input B).

suspension was heated at 110 °C, and then about 7 mL of solvent was distilled and collected in the trap to remove the adsorbed water. After this step, the mixture was stirred for 24 h at room temperature to load the dye into the MS-face pores. Afterward, an excess of 3-iodopropyltrimethoxysilane (200 μL, 1 mmol) was added, and the suspension was stirred for 24 h.[7f] The final solid was filtered off, washed two times with 5 mL of acetonitrile, and dried at 60 °C overnight. To attach the benzimidazole moieties to the MS surface, 400 mg of the resulting solid was suspended in a 40 mL of a saturated solution of benzimidazole in toluene at 80 °C and containing triethylamine (benzimidazole and triethylamine in 1:3 proportion). The suspension was refluxed and stirred for 72 h. The resulting solid was filtered off, washed with 40 mL of acetonitrile, and dried at 70 °C overnight.

dx.doi.org/10.1021/ja503578b | J. Am. Chem. Soc. 2014, 136, 9116−9123

Preparation of S3, S4, and S5. To prepare the gated solid **S3**, 400 mg of **S2** was suspended in 100 mL of a β-cyclodextrin solution (1.6 mg/mL) in 50 mM sodium phosphate buffer, pH 7.5.[7f] The suspension was stirred for 12 h at room temperature. The capped solid was centrifuged, washed with water at pH 7.5, and dried. In a second step, to functionalize these nanoparticles with the enzymes, 2.0 mg of enzyme (esterase or glucose oxidase) and 2.0 mg of 3,3′-dithiobis-(sulfosuccinimidylpropionate) were dissolved in 2.0 mL of 50 mM sodium phosphate buffer, pH 7.0, and stirred for 2 h at 4 °C.[9] Afterward, 200 μL of 100 mM $NaBH_4$ solution was added, and the mixture was stirred at 4 °C for 30 min. The solution was exhaustively dialyzed vs 50 mM sodium phosphate buffer, pH 7.0, using Amicon Ultra-05 centrifugal filter units with Ultracel-10 membranes (Millipore, USA), and finally concentrated to about 10 mg/mL. The modified enzyme solutions were then added to 20 mL of 50 mM sodium phosphate buffer, pH 7.5, containing 20 mg of the β-cyclodextrin-capped solid, and stirred at 4 °C overnight. The resulting solid (**S3**) was finally isolated by centrifugation, washed several times with a cold solution of 50 mM sodium phosphate buffer, pH 7.5, dried, and kept in a refrigerator until use. Solid **S4** was prepared through a similar protocol, but co-immobilizing a third enzyme, urease, on the Au nanoparticles surface. For *ex vivo* cell experiments, nanoparticles like **S3** but loaded with the cytotoxic doxorubicin were also prepared (solid **S5**, see SI).

Cell Culture Conditions. HeLa human cervix adenocarcinoma cells were purchased from the German Resource Centre for Biological Materials (DSMZ) and were grown in DMEM supplemented with 10% FBS. Cells were maintained at 37 °C in an atmosphere of 5% carbon dioxide and 95% air and underwent passage twice a week.

WST-1 Cell Viability Assay. HeLa cells were seeded in a 24-well plate at a density of 2×10^4 cells/well in 1000 μL of DMEM and were incubated 24 h in a CO_2 incubator at 37 °C. Then, DMEM was replaced with PBS with 10% FBS, and solid **S5** in DMSO was added to cells in sextuplicate at final concentrations of 150 μg/mL. After 40 min, the cells were washed with PBS and then incubated for 23 h in different conditions: DMEM with 10% FBS, DMEM with 10% FBS and ethyl butyrate, PBS with 10% FBS, or PBS with 10% FBS and ethyl butyrate. After this, 35 μL of WST-1 was added to each well and incubated for 1.5 h. Before readings, the plate was shaken for 1 min to ensure homogeneous distribution of color. The absorbance was then measured at a wavelength of 450 nm in a PerkinElmer VICTOR X5 multilabel plate reader. Results are expressed as an average of the results of six independent experiments obtaining similar results.

Live Confocal Microscopy. HeLa cells were seeded in 24 mm diameter glass coverslips in six-well plates at a seeding density of 1.8×10^5 cells/well. After 24 h, the culture medium was replaced with PBS with 10% FBS, and cells were treated with a suspension of solid **S5** for 40 min at a final concentration of 100 μg/mL. The medium was changed for different solutions (DMEM with 10% FBS with or without ethyl butyrate, or PBS with 10% FBS with or without ethyl butyrate). After 18 h, coverslips were washed twice to eliminate compounds and visualized under a Leica TCS SP2 AOBS inverted laser scanning confocal microscope (Leica Microsystems Heidelberg GmbH, Mannheim, Germany) using oil objectives: 63X Plan-Apochromat-Lambda Blue 1.4 N.A. The images were acquired with an excitation wavelength of 405 nm for Hoescht and 480 nm for doxorubicin. Two-dimensional pseudo-color images (255 color levels) were gathered with a size of 1024 × 1024 pixels and Airy 1 pinhole diameter. All confocal images were acquired using the same settings, and the distribution of fluorescence was analyzed using ImageJ Software. Three fields of each condition in two independent experiments gave similar results.

■ ASSOCIATED CONTENT

Supporting Information

Experimental details and nanomaterials characterization. This material is available free of charge via the Internet at http://pubs.acs.org.

■ AUTHOR INFORMATION

Corresponding Authors

rmaez@qim.upv.es
rvillalonga@quim.ucm.es
pingarro@quim.ucm.es

Notes

The authors declare no competing financial interest.

■ ACKNOWLEDGMENTS

R.V. acknowledges a Ramón & Cajal contract from the Spanish Ministry of Science and Innovation. Financial support from the Spanish Ministry of Science and Innovation (CTQ2011-24355, CTQ2009-12650, CTQ2009-09351, MAT2012-38429-C04-01) and Comunidad de Madrid (S2009/PPQ-1642, programme AVANSENS) is gratefully acknowledged. The Generalitat Valencia (project PROMETEO/2009/016) is also acknowledged.

■ REFERENCES

(1) (a) Ozin, G. A. *Adv. Mater.* **1992**, *4*, 612−649. (b) Katz, E.; Willner, I. *Angew. Chem., Int. Ed.* **2004**, *43*, 6042−6108.

(2) (a) Allen, T. M.; Cullis, P. R. *Science* **2004**, *303*, 1818−1822. (b) Valdivia, A.; Perez, Y.; Dominguez, A.; Caballero, J.; Gomez, L.; Schacht, E. H.; Villalonga, R. *Macromol. Biosci.* **2005**, *5*, 118−123. (c) Allen, T. M.; Cullis, P. R. *Adv. Drug Delivery Rev.* **2013**, *65*, 36−48. (d) Ramírez, H. L.; Valdivia, A.; Cao, R.; Torres-Labandeira, J. J.; Fragoso, A.; Villalonga, R. *Bioorg. Med. Chem. Lett.* **2006**, *16*, 1499−1501.

(3) (a) Brannon-Peppas, L.; Blanchette, J. O. *Adv. Drug Delivery Rev.* **2012**, *64*, 206−212. (b) Doane, T. L.; Burda, C. *Chem. Soc. Rev.* **2012**, *41*, 2885−2911. (c) Wang, A. Z.; Langer, R.; Farokhzad, O. C. *Annu. Rev. Med.* **2012**, *63*, 185−198.

(4) (a) Tang, F.; Li, L.; Chen, D. *Adv. Mater.* **2012**, *24*, 1504−1534. (b) Li, Z.; Barnes, J. C.; Bosoy, A.; Stoddart, J. F.; Zink, J. I. *Chem. Soc. Rev.* **2012**, *41*, 2590−2605.

(5) (a) Coll, C.; Bernardos, A.; Martínez-Máñez, R.; Sancenón, F. *Acc. Chem. Res.* **2013**, *46*, 339−349. (b) Cotí, K.; Belowich, M. E.; Liong, M.; Ambrogio, M. W.; Lau, Y. A.; Khatib, H. A.; Zink, J. I.; Khashab, N. M.; Stoddart, J. F. *Nanoscale* **2009**, *1*, 16−39. (c) Yang, P.; Gai, S.; Lin, J. *Chem. Soc. Rev.* **2012**, *41*, 3679−3698.

(6) (a) Mal, N. K.; Fujiwara, M.; Tanaka, Y. *Nature* **2003**, *421*, 350−353. (b) Aznar, E.; Mondragón, L.; Ros-Lis, J. V.; Sancenón, F.; Marcos, M. D.; Martínez-Máñez, R.; Soto, J.; Pérez-Payá, E.; Amorós, P. *Angew. Chem., Int. Ed.* **2011**, *50*, 11172−11175.

(7) See, for example: (a) Lai, C. Y.; Trewyn, B. G.; Jeftinija, D. M.; Jeftinija, K.; Xu, S.; Jeftinija, S.; Lin, V. S. Y. *J. Am. Chem. Soc.* **2003**, *125*, 4451−4459. (b) Park, C.; Oh, K.; Lee, S. C.; Kim, C. *Angew. Chem., Int. Ed.* **2007**, *46*, 1455−1457. (c) Casasús, R.; Climent, E.; Marcos, M. D.; Martínez-Máñez, R.; Sancenón, F.; Soto, J.; Amorós, P.; Cano, J.; Ruiz, E. *J. Am. Chem. Soc.* **2008**, *130*, 1903−1917. (d) Liu, R.; Liao, P.; Liu, J.; Feng, P. *Langmuir* **2011**, *27*, 3095−3099. (e) Zhao, Z.; Meng, H.; Wang, N.; Donovan, M. J.; Fu, T.; You, M.; Chen, Z.; Zhang, X.; Tan, W. *Angew. Chem., Int. Ed.* **2013**, *52*, 7487−7491. (f) Aznar, E.; Villalonga, R.; Giménez, C.; Sancenón, F.; Marcos, M. D.; Martínez-Máñez, R.; Díez, P.; Pingarrón, J. M.; Amorós, P. *Chem. Commun.* **2013**, *49*, 6391−6393.

(8) See, for example: (a) Patel, K.; Angelos, S.; Dichtel, W. R.; Coskun, A.; Yang, Y. W.; Zink, J. I.; Stoddart, J. F. *J. Am. Chem. Soc.* **2008**, *130*, 2382−2383. (b) Schlossbauer, A.; Kecht, J.; Bein, J. *Angew. Chem., Int. Ed.* **2009**, *48*, 3092−3095. (c) Park, C.; Kim, H.; Kim, S.; Kim, C. *J. Am. Chem. Soc.* **2009**, *131*, 16614−16615.

(9) Villalonga, R.; Díez, P.; Sánchez, A.; Aznar, E.; Martínez-Máñez, R.; Pingarrón, J. M. *Chem.—Eur. J.* **2013**, *19*, 7889−7894.

(10) (a) Perro, A.; Reculusa, S.; Ravaine, S.; Bourgeat-Lami, E.; Duguet, E. J. *J. Mater. Chem.* **2005**, *15*, 3745−3760. (b) Jiang, S.;

Chen, Q.; Tripathy, M.; Luijten, E.; Schweizer, K. S.; Granick, S. *Adv. Mater.* **2010**, *22*, 1060−1071.
(11) Du, L.; Liao, S.; Khatib, H. A.; Stoddart, J. F.; Zink, J. I. *J. Am. Chem. Soc.* **2009**, *131*, 15136−15142.
(12) (a) Tokarev, I.; Gopishetty, V.; Zhou, J.; Pita, M.; Motornov, M.; Katz, E.; Minko, S. *ACS Appl. Mater. Interfaces* **2009**, *1*, 532−536. (b) Du, L.; Liao, S.; Khatib, H. A.; Stoddart, J. F.; Zink, J. I. *J. Am. Chem. Soc.* **2009**, *131*, 15136−15142.
(13) Sánchez, A.; Díez, P.; Martínez-Ruíz, P.; Villalonga, R.; Pingarrón, J. M. *Electrochem. Commun.* **2013**, *30*, 51−54.
(14) Leff, D. V.; Brandt, L.; Heath, J. R. *Langmuir* **1996**, *12*, 4723−4730.
(15) Mohan, S.; Sundaraganesan, N.; Mink, J. *Spectrochim. Acta Mol. Biomol. Spectros.* **1991**, *47*, 1111−1115.
(16) Jerez, G.; Kaufman, G.; Prystai, M.; Schenkeveld, S.; Donkor, K. K. *J. Sep. Sci.* **2009**, *32*, 1087−1095.
(17) (a) Tsuge, H.; Natsuaki, O.; Ohashi, K. *J. Biochem.* **1975**, *78*, 835−843. (b) Junge, W.; Heymann, E. *Eur. J. Biochem.* **1979**, *95*, 519−525.
(18) Zhao, Y.; Trewyn, B. G.; Slowing, I. I.; Lin, V. S. Y. *J. Am. Chem. Soc.* **2009**, *131*, 8398−8400.
(19) Frens, G. *Nature* **1973**, *241*, 20−22.